

Structures of segments of α -synuclein fused to maltose-binding protein suggest intermediate states during amyloid formation

Minglei Zhao,^{1,2} Duilio Cascio,^{1,2,3} Michael R. Sawaya,^{1,2,3}
and David Eisenberg^{1,2,3*}

¹Department of Biological Chemistry, David Geffen School of Medicine, University of California, Los Angeles, California 90095

²Howard Hughes Medical Institute, UCLA-DOE Institute of Genomics and Proteomics, University of California, Los Angeles, California 90095

³Department of Chemistry and Biochemistry, University of California, Los Angeles, California 90095

Received 4 February 2011; Revised 18 March 2011; Accepted 22 March 2011

DOI: 10.1002/pro.630

Published online 1 April 2011 proteinscience.org

Abstract: Aggregates of the protein α -synuclein are the main component of Lewy bodies, the hallmark of Parkinson's disease. α -Synuclein aggregates are also found in many human neurodegenerative diseases known as synucleinopathies. *In vivo*, α -synuclein associates with membranes and adopts α -helical conformations. The details of how α -synuclein converts from the functional native state to amyloid aggregates remain unknown. In this study, we use maltose-binding protein (MBP) as a carrier to crystallize segments of α -synuclein. From crystal structures of fusions between MBP and four segments of α -synuclein, we have been able to trace a virtual model of the first 72 residues of α -synuclein. Instead of a mostly α -helical conformation observed in the lipid environment, our crystal structures show α -helices only at residues 1–13 and 20–34. The remaining segments are extended loops or coils. All of the predicted fiber-forming segments based on the 3D profile method are in extended conformations. We further show that the MBP fusion proteins with fiber-forming segments from α -synuclein can also form fiber-like nano-crystals or amyloid-like fibrils. Our structures suggest intermediate states during amyloid formation of α -synuclein.

Keywords: α -synuclein; amyloid; fibrillation; intermediate; MBP fusion; nano-crystal; X-ray crystallography

Introduction

α -synuclein is a neuronal protein involved in many human neurodegenerative diseases, for example,

Abbreviations: EM, electron microscopy; EPR, electron paramagnetic resonance; IAPP, islet amyloid polypeptide; MBP, maltose-binding protein; NAC, non-A β component; NMR, nuclear magnetic resonance; SDS, sodium dodecyl sulfate.

Additional Supporting Information may be found in the online version of this article.

Grant sponsors: NIH, NSF, DOE.

*Correspondence to: David Eisenberg, Howard Hughes Medical Institute, UCLA-DOE Institute for Genomics and Proteomics, Los Angeles, CA 90095-1570. E-mail: david@mbi.ucla.edu

Parkinson's disease (PD), multiple system atrophy (MSA), and dementia with Lewy bodies (DLB).^{1–4} A common feature in these diseases is that α -synuclein forms insoluble filamentous inclusions known as Lewy bodies in patients' neuronal tissues. The term synucleinopathies was introduced to encompass all diseases involving α -synuclein deposition.^{5–8}

In vitro, α -synuclein has been shown to be unfolded in aqueous solution and to be α -helical or β -structural in apolar organic solvents.⁹ In a lipid environment, for example, in the presence of lipid vesicles¹⁰ or detergent micelles,¹¹ most residues of the protein are in α -helical conformations. The function of α -synuclein has not been fully defined, but

current evidence points to vesicle trafficking regulation where α -synuclein associates with membranes and interacts with SNARE complexes.^{12–14} Therefore, in this study, we refer to the membrane-bound α -helical conformation as a native-like reference state of α -synuclein. In diseases, α -synuclein forms typical amyloid fibrils, with a cross- β diffraction pattern indicating that β -sheet containing structures predominate.^{15,16} How the protein converts from the functional α -helix-rich state to the pathological β -sheet-rich amyloid state is important for understanding the cause of the diseases and to search for possible cures.

The structure of α -synuclein, both in the membrane-bound state and in the amyloid state, has been extensively studied by solution NMR,¹¹ solid state NMR,^{17,18} electron paramagnetic resonance (EPR),^{10,19,20} and X-ray crystallography.²¹ Ulmer *et al.* provided the first full-length atomic model of α -synuclein in SDS micelles using solution NMR. The first 93 residues form two anti-parallel helices with a turn spanning residues 37–44.¹¹ Jao *et al.* showed that in the presence of synthetic lipid vesicles the first 90 residues form a continuous long α -helix using EPR.²⁰ Together with the follow-up studies,^{22–24} they suggested that the helix conformation is largely dependent on the shape and makeup of the lipid. EPR was also used to characterize α -synuclein fibrils, showing that residues 36–98 constitute a parallel, in-register core.¹⁹ Solid state NMR also provided valuable information of the arrangement of β strands in the amyloid state.^{17,18} Atomic resolution of the fibrils was partially achieved by crystallizing short fiber-forming segments of α -synuclein (Ivanova *et al.*, unpublished data), but a full-length model of α -synuclein fibril is not yet available. The only crystal structure of α -synuclein in Protein Data Bank is a complex of α -synuclein C-terminal peptide with a single domain camelid antibody fragment,²¹ in which the last six residues (¹³⁵DYE-PEA¹⁴⁰) of α -synuclein are modeled.

Progress has been made in structural characterization of α -synuclein in the membrane-bound state as well as in the amyloid state. However, structural information regarding the transition is very limited.²⁵ Here, we present our crystallographic studies on segments of α -synuclein. We used maltose-binding protein (MBP) as a carrier to crystallize four segments of α -synuclein, which in total correspond to the first 72 residues. The crystal structures reveal a combination of α -helices, extended loops and coils, suggesting an intermediate between the α -helix-rich membrane-bound conformation and the β -sheet rich amyloid conformation. To test this hypothesis, we carried out fibrillation experiments with the fusion proteins and showed that they can form fiber-like nano-crystals or amyloid-like fibrils after incubation. Our study suggests a possible application of crystal-

lography for characterizing intermediate structures of amyloid proteins.

Results

Prediction of fiber-forming segments in α -synuclein

Human α -synuclein has 140 residues, with seven 11-mer repeats (denoted R1–R7) and an acidic C-terminal tail [Fig. 1(A)]. One of the repeats, R6, is less similar to the others [Fig. 1(B)]. R6 is within the NAC (non-A beta component) region of α -synuclein.²⁹ We used the 3D profile computer algorithm^{26,28} to identify fiber-forming segments of α -synuclein [Fig. 1(C)]. This algorithm scores successive, overlapping six-residue segments by their Rosetta energy²⁷ in a structural profile of a canonical steric zipper.³⁰ Energy-favored hits were found at three regions of α -synuclein: residues 14–20 within R1, residues 47–56 within R4, and residues 67–95 corresponding to the NAC region. Except the two hits close to the N-terminus (residues 14–20), the predictions are in agreement with EPR and solid state NMR data that have suggested the core of α -synuclein fibrils.^{17–19}

Crystal structures of α -synuclein segments fused to MBP

We first attempted to crystallize full-length α -synuclein with MBP as a carrier, but the longest crystallizable construct turned out to be the first 42 residues fused to MBP. Unfortunately, the density of α -synuclein was not traceable for that particular construct. Other fusion proteins that we tested, formed from α -synuclein segments fused to the C-terminus of MBP, are summarized in Table I. Among the crystallized fusion proteins, four showed traceable electron density of α -synuclein and are presented here: MBP- α S_{1–19}, MBP- α S_{10–42}, MBP- α S_{32–57}, and MBP- α S_{58–79} [Fig. 2(A) and Table II].

The fusion of MBP- α S_{1–19} starts from residue 1 and ends right before R1. All 19 residues were observed in clear density with the first 13 residues in α -helical conformations. Residues 14–19 (¹⁴GVVAAA¹⁹), which are predicted to be a fiber-forming segment, form an extended strand [Fig. 2(A) upper left panel]. Interestingly in another crystal form of the same construct (Supporting Information Fig. S1, PDB code 3Q29) the segment (14–19) is not traceable. The fact that this segment is either extended or disordered instead of being α -helical as in the presence of detergents (PDB code 1XQ8¹¹) suggests that our crystal structure reflects a state intermediate between the native α -helices and amyloid fibrils.

The fusion of MBP- α S_{10–42} starts from R1 and ends at R3. Residues 12–19 of R1 are disordered and residues 20–42 corresponding to R2 and R3 are traceable. Residues 20–34 form an α -helix and

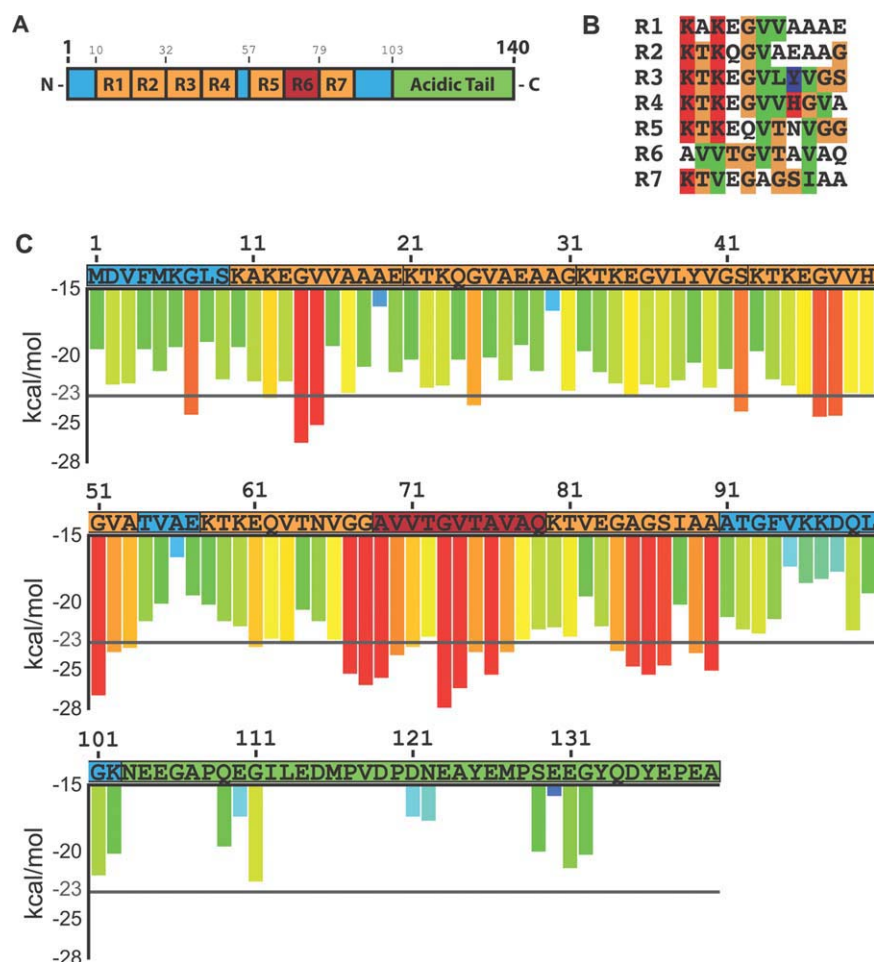


Figure 1. Domain architecture of α -synuclein and prediction of fiber-forming segments by the 3D profile method. A: Domain architecture of α -synuclein. The seven 11-mer repeats are colored in orange and red, with red highlighting R6, the repeat that is less similar to the other repeats. The C-terminal acidic tail is in green. All other segments are in blue. B: Sequence comparison of the seven 11-mer repeats of α -synuclein. Residues are colored as follows: basic, red; aromatic, blue; polar, yellow; non-polar, green. C: Prediction of fiber-forming segments by the 3D profile method.²⁶ The Rosetta energy²⁷ of steric zipper-like self-association was calculated by scanning through the sequence with a six-residue window. The energy was not calculated if the window included a proline. Energies below -23 kcal/mol (indicated by a gray line) are likely to form amyloid-like fibrils according to previous experience.²⁸ The calculated energies of segments are colored in rainbow from blue to red for low to high predicted propensity for fiber formation. Above the histogram, the sequence of α -synuclein is colored as the domain diagram in (A).

residues 35–42 form an extended loop [Fig. 2(A) lower left panel]. The predicted fiber-forming segment in R1, ¹⁴GVVAAA¹⁹, is disordered and cannot be seen in the electron density map.

The fusion of MBP- α S₃₂₋₅₇ starts from R3 and ends before R5. The first 5 residues of R3 are not traceable and the remaining residues form a coiled loop with several turns. The predicted fiber-forming region in R4 starts at G47, which is indicated by a red arrow [Fig. 2(A) upper right panel].

The fusion of MBP- α S₅₈₋₇₉ starts from R5 and ends at R6. The last seven residues (73–79) are not traceable. The structure constitutes two extended loops connected by a right angle turn where the predicted fiber-forming region starts [Fig. 2(A) lower right]. The traceable fiber-forming segment (⁶⁷GGAVVT⁷²) appears as an extended strand.

In all fusion structures, α -synuclein segments extend out of the globular MBP and interact with symmetry related MBP molecules [Fig. 2(B)]. Combining four crystal structures, we can trace the first 72 residues of α -synuclein, except residue E57. Modeled regions from the four structures are almost continuous with the only overlap being at residues 37–42 from MBP- α S₁₀₋₄₂ and MBP- α S₃₂₋₅₇ (Supporting Information Fig. S2). Twenty-eight out of 72 residues (1–13, 20–34) are in α -helical conformations, in contrast to 65 out of 72 residues being α -helical in the presence of SDS micelles.¹¹ The remaining residues form various loops and turns, indicating structural flexibility of α -synuclein. Four out of five predicted fiber-forming segments are in extended loops. The one exception is ⁵¹GVATVA⁵⁶, which forms a coiled loop. Apparently, these segments are capable

Table I. Summary of Fusion Constructs of Maltose-Binding Protein (MBP) with α -Synuclein

Segments of α -synuclein fused to MBP	EM observations after fibrillation	Space groups of crystals
1–19 ^a	Fiber-like nano-crystals	$P4_32_12$, $P2_12_12_1$, ^b
1–42	Nano-crystals	$P2_1$
1–57	Fiber-like nano-crystals	No crystals
1–79	Fibers	No crystals
1–100	Fibers	No crystals
1–140	Fibers	No crystals
21–42	Nano-crystals	$P2_1$
32–57 ^a	Fiber-like nano-crystals	$P2_1$
58–79 ^a	Fiber-like nano-crystals	$P2_1$
10–42 ^a	Fiber-like nano-crystals	$P2_12_12_1$
21–57	Fiber-like nano-crystals	$P2_12_12_1$
32–57	Fiber-like nano-crystals	$P2_12_12_1$
32–79	Fiber-like nano-crystals	$P2_12_12_1$
43–79	Fiber-like nano-crystals	$P2_12_12_1$

^a Structures showed traceable density of α -synuclein.

^b Structure of MBP- α S₁₋₁₉ crystallized in space group $P2_12_12_1$ is shown in Supporting Information Figure S1, PDB code 3Q29.

of fiber formation, but the MBP isolates them from identical segments, with which they could form self-complementary steric zipper structures. In the absence of these self-interactions, they take up extended or coiled conformations.

Fibrillation of the fusion proteins

To test whether the crystal structures reflect an intermediate state during fibrillation of α -synuclein, we conducted fibrillation experiments with each of our fusion proteins as well as with the controls of wild type MBP and α -synuclein. Thioflavin T, which fluoresces when bound to amyloid fibrils, was incubated with each construct, shaken at 37°C and fluorescence was monitored as a function of time (Fig. 3). As expected, wild type α -synuclein showed a typical nucleation dependent kinetic curve with a lag time around 5 h. Wild type MBP did not show any fluorescence, but fusion proteins with full-length α -synuclein (MBP- α S₁₋₁₄₀) and the first 79 residues of α -synuclein (MBP- α S₁₋₇₉) did. The lag time of the two fusion proteins were 90 and 60 h, respectively, much longer than that of wild type α -synuclein, showing that the fused, globular MBP slows fibrillation. MBP- α S₁₋₇₉ was the shortest construct that could recapitulate typical thioflavin T (ThT) fluorescence of amyloid in our fibrillation experiments. None of the other fusion constructs tested showed fluorescence (Fig. 3).

To validate the presence of amyloid-like fibrils from the fibrillation experiments, we examined all samples by negative-stain EM after 2 weeks of incubation (Fig. 4). As expected, wild type α -synuclein and MBP- α S₁₋₇₉ showed typical unbranched amyloid-like fibrils [Fig. 4(B) lower panels]. The four

crystallized constructs, without visible ThT fluorescence, showed fiber-like nano-crystals that are much thicker than typical amyloid fibrils [Fig. 4(A)], but

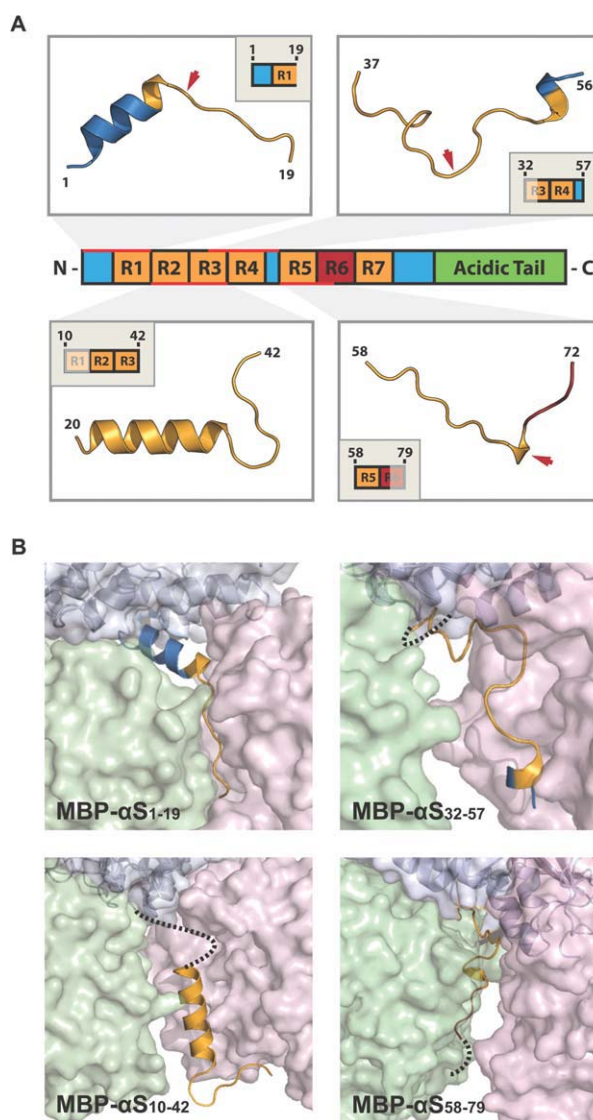


Figure 2. Crystal structures of segments of α -synuclein fused to MBP. A: Four MBP- α -synuclein fusion constructs were crystallized. Structures of the α -synuclein segment in each crystal are shown as cartoon representations in four boxes, which are mapped to a domain diagram based on traceable residues (highlighted by red bars). In each box, the starting and ending residues are numbered according to the wild type human α -synuclein sequence. The insets show domain diagrams of the actual fused segments with untraceable parts shadowed. The models are colored according to the domain diagram. Red arrows point at the start of predicted fiber-forming regions. B: Close-up views of α -synuclein segments in their crystal structures. Surface representations of three crystallographic symmetry-related MBP molecules are shown in each picture. They are colored blue white, pale green, and light pink. Only the α -synuclein segment that belongs to the blue white MBP molecule is shown in cartoon representation and is colored the same as in (A). The missing parts of α -synuclein segments are denoted by dashed lines.

Table II. X-Ray Data Collection and Refinement Statistics for MBP α -Synuclein Fusion Structures

	MBP- α S ₁₋₁₉	MBP- α S ₁₀₋₄₂	MBP- α S ₃₂₋₅₇	MBP- α S ₅₈₋₇₉
Crystal parameters				
Space group	<i>P</i> _{4₃2₁2}	<i>P</i> _{2₁2₁2₁}	<i>P</i> _{2₁}	<i>P</i> _{2₁}
Cell dimensions				
a, b, c (Å)	77.47, 77.47, 172.64	48.74, 57.49, 127.23	57.51, 49.95, 59.34	57.54, 48.57, 57.85
α, β, γ (°)	90, 90, 90	90, 90, 90	90, 92.19, 90	90, 94.22, 90
Data collection				
Synchrotron beamline	APS (24-ID-E)	APS (24-ID-C)	APS (24-ID-C)	APS (24-ID-C)
Wavelength (Å)	0.9791	0.9795	0.9795	0.9795
Resolution range (Å)	70.7–1.90	63.6–1.54	59.3–1.30	19.6–1.60
Reflections observed/unique	328790/42116	412260/53765	507911/82058	571250/42173
Completeness (%)	99.5 (100) ^a	100 (99.9)	99.6 (99.9)	99.9 (100)
R_{merge} (%) ^b	5.1 (55.7)	7.7 (56.1)	7.8 (56.8)	8.3 (55.7)
$\langle I/\sigma I \rangle$	25.3 (4.5)	17.7 (3.6)	16.1 (2.8)	22.7 (4.0)
Refinement				
Resolution (Å)	37.8–1.90	63.6–1.54	59.3–1.30	19.6–1.60
$R_{\text{work}}/R_{\text{free}}$ (%) ^c	17.0/19.6	14.0/18.3	13.1/15.6	15.2/17.3
No. atoms				
Protein	3004	3121	3056	3029
Ligand/ion	109	97	73	66
Water	279	388	471	310
<i>B</i> -factors				
Overall	36	14	18	18
Protein	35	13	16	17
Solvent	45	27	31	27
R.m.s. deviation				
Bond length (Å)	0.006	0.009	0.007	0.008
Bond angle (°)	0.947	1.180	1.164	1.118
Ramachandran map				
Favored (%)	96.8	96.7	96.2	95.6
Allowed (%)	2.9	3.0	3.5	4.1
Outliers (%)	0.26	0.27	0.27	0.27
PDB accession code	3Q25	3Q26	3Q27	3Q28

^a Values in parentheses correspond to the highest resolution shell.

^b $R_{\text{merge}} = \sum |I - \langle I \rangle| / \sum I$.

^c $R_{\text{work}} = \sum |F_o - F_c| / \sum F_o$. $R_{\text{free}} = \sum |F_o - F_c| / \sum F_o$, calculated using a random set containing 5% reflections that were not included throughout structure refinement.

are reminiscent of nano-crystals that we have observed for other fiber-forming segments.^{30–32} MBP without α -synuclein fusion did not fibrillize or form nano-crystals [Fig. 4(B) upper left]. Therefore, the nano-crystals result from the fusion of MBP to α -synuclein segments. Nano-crystals were also observed for MBP- α S₂₁₋₄₂, but they were not fiber-like [Fig. 4(B) upper right]. This may be due to the fact that the fusion of MBP- α S₂₁₋₄₂ starts at R2 and ends at R3, which does not include any fiber-forming segments [Fig. 1(C)].

Discussion

MBP fusion has been successfully applied to crystallize numerous proteins that were otherwise resistant to forming X-ray grade crystals.³³ One such application is to proteins that would otherwise enter the amyloid state. With both human IAPP³⁴ and the N-terminus of human huntingtin,³⁵ MBP fusions have suggested intermediate states of each protein before amyloid formation. That is, MBP fusions permit structure determination in the absence of identical segments of the amyloid-forming protein that would

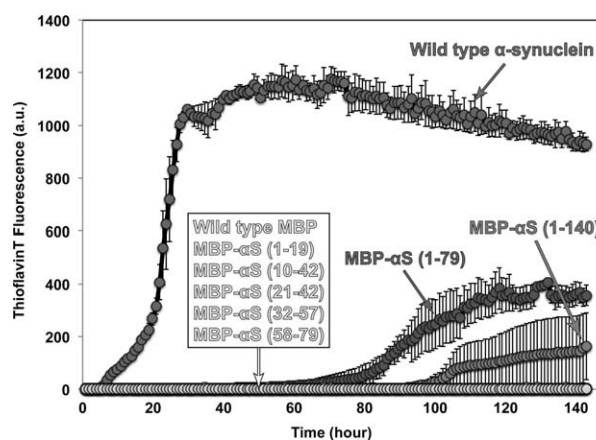


Figure 3. The kinetics of fibrillation of MBP- α -synuclein fusion proteins followed by thioflavin T fluorescence. Thioflavin T fluorescence was monitored over 2 weeks for seven MBP- α -synuclein fusion proteins as well as for wild type MBP and α -synuclein. The kinetic curves for the first 140 h are shown. Only three proteins showed significant fluorescence. The trend did not change after 140 h until the end of the experiment. No fluorescence signal was observed for wild type MBP, MBP- α S₁₋₁₉, MBP- α S₁₀₋₄₂, MBP- α S₂₁₋₄₂, MBP- α S₃₂₋₅₇, and MBP- α S₅₈₋₇₉.

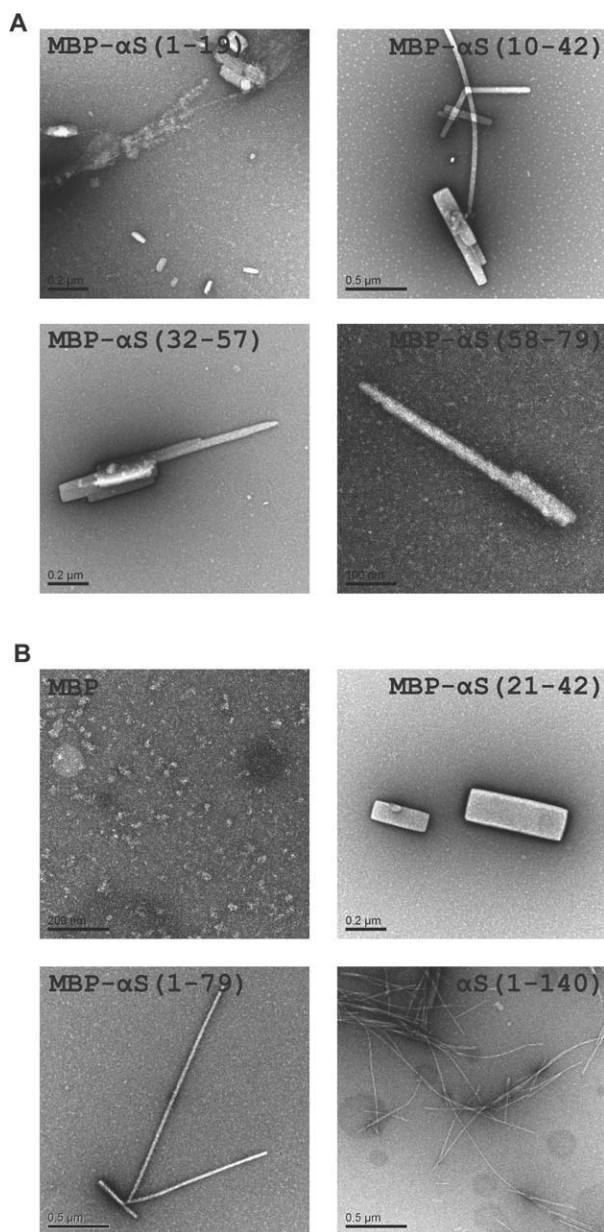


Figure 4. Electron micrographs of MBP- α -synuclein fusion proteins after the fibrillation experiment. A: Electron micrographs of the four fusion proteins whose crystal structures are reported in this paper. B: Electron micrographs of: wild type MBP as a negative control, wild type α -synuclein as a positive control, MBP- α S₁₋₇₉, which is the shortest construct showing typical amyloid-like fibrils, and MBP- α S₂₁₋₄₂, which does not have any predicted fiber-forming segments in its fused sequence. Scale bars are given in each micrograph.

otherwise cause fibrillation. The crystal acts as an isolation chamber, bathed in a polar medium that does not necessarily promote α -helix formation, allowing the preamyloid segment to take up a favored conformation in the absence of binding proteins. This favored conformation may reflect the structure that is intermediate between the all α -helical native-like structure and the all β -sheet, fibrillar

structure. A caveat in interpreting the structure of these preamyloid segments is that its conformation can be influenced by interactions with its own MBP fusion partner or other MBP molecules in the crystal.

As shown in Table I and Figure 2, we crystallized four MBP- α -synuclein fusion constructs and were able to trace the first 72 residues of α -synuclein from the four structures. Figure 5 shows a composite model, pieced together from these four crystal structures. All fiber-forming segments predicted by the 3D profile method were found in loops rather than in fiber-like structures. This is as expected because no identical segments are available in proximity in the crystal structures. However, when the MBP fusions were incubated for fibrillation, nano-crystals were observed, typical of fiber-forming segments reported before.³⁰⁻³² This shows that the fiber-forming segments are capable of forming fibers. We, therefore, refer to them as prefiber-forming segments.

In our fusion crystal structures, α -synuclein segments form some interactions with symmetry-related MBP molecules, but their conformations do not appear to be determined by these interactions [Fig. 2(B)]. The two α -helices (residues 1-13 and 20-34) form hydrogen bonds to either water or MBP molecules mainly through their side chains. The conformations of the loop regions (residues 14-19 and 35-72) appear to be maintained mainly through backbone hydrogen bonds to water molecules: among a total of 60 intermolecule hydrogen bonds, 47 are backbone hydrogen bonds and 32 out of 47 are to water molecules. This suggests that the conformations of the loop regions are not completely determined by MBP molecules, and therefore may reflect an intrinsic propensity of residues 14-19 and 35-72 to be flexible and extended in a polar medium. When the prefiber-forming segments in these regions are freely exposed in similar solution conditions, and when self-association is not prevented by crystal packing, amyloid-like fibrils will form as observed in our fibrillation experiments. Our structures also suggest that residues 1-13 and 20-34 are less flexible and tend to maintain native α -helical conformations in the polar medium. The higher propensity of the first 30 residues to maintain α -helix conformation in a lipid medium was demonstrated by NMR.³⁶

It is known that many proteins interact with α -synuclein *in vivo*.^{1,37-40} Our crystal structures may also represent such an "interacting state" of α -synuclein. Although in our crystals α -synuclein segments interact with bacteria MBP [Fig. 2(B)], which is biologically irrelevant, these interactions may offer insight into the way that the synuclein molecule can convert to a partially opened conformation, permitting interactions of some of its segments with

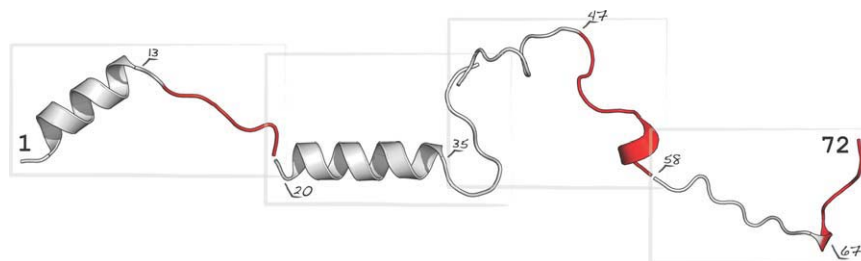


Figure 5. A composite model of the first 72 residues of α -synuclein. The model was pieced together from four crystal structures outlined in boxes. Predicted fiber-forming segments are colored red. Residues at the boundary of α -helices and fiber-forming segments are labeled. The model represents a partially opened intermediate state of α -synuclein.

various other protein partners, whereas other segments of α -synuclein maintain protected α -helical conformations.

Intermediate states of amyloid proteins are important for understanding the initiation of fibrillation and the etiology of disease. In our fusion crystals, the packing of the MBP molecules prevents self-association of the fiber-forming segments in α -synuclein, thereby trapping intermediate states. When linked together, these intermediate states are suggestive of a partially opened conformation that could exist during amyloid formation and also during the formation of interactions of α -synuclein with other proteins.

Materials and Methods

Plasmid construction, protein expression, and purification

All α -synuclein segments were cloned into pMAL-c2X vector (New England Biolabs, Ipswich, MA) between *SacI* and *SalI* sites, which left a three-residue linker (³⁶⁹SSS³⁷¹) between MBP and each synuclein segment. The fusion proteins were expressed in BL21-Gold (DE3) competent cells (Agilent Technologies, Santa Clara, CA). Proteins were purified by affinity chromatography, followed by gel filtrations. Detailed procedures are described in Supporting Information.

Crystallization, data collection, and structure determination

All crystals of fusion proteins were obtained using hanging drop vapor diffusion method. Crystals were grown at 18°C for a week before cryoprotection and flash freezing in liquid nitrogen. X-ray diffraction data were collected at the Advanced Photon Source (APS). Reflections were integrated and scaled using either DENZO/SCALEPACK⁴¹ or XDS/XSCALE⁴² program packages. Molecular replacement was performed using the CCP4 program PHASER^{43,44} with PDB model 1ANF. The models were built manually using COOT⁴⁵ and were refined using PHENIX.⁴⁶ Coordinates and structure factor amplitudes have

been deposited in the PDB with accession code 3Q25, 3Q26, 3Q27, 3Q28, and 3Q29. Detailed crystallization conditions are provided in Supporting Information.

Electron microscopy

Samples of 5 μ L volume were spotted directly on freshly glow-discharged carbon-coated electron microscopy grids (Ted Pella, Redding, CA). After 3 min incubation, grids were rinsed twice with 5- μ L distilled water and stained with 1% uranyl acetate for 1 min. Specimens were examined in a JEM1200-EX electron microscope at an accelerating voltage of 80 kV. Images were recorded digitally by wide angle (top mount) BioScan 600W 1 \times 1K digital camera (Gatan, Pleasanton, CA).

Fibrillation assay

Proteins at a concentration of 200 μ M were incubated in a buffer containing 20 mM Tris-HCl (pH 8.0), 100 mM NaCl, 10 mM maltose, and 10 μ M thioflavin T, with constant shaking (900 rpm, 1 mm diameter) at 37°C for 2 weeks. All reactions were conducted in a 96-well plate with a total volume of 150 μ L for each reaction and were monitored in a Varioskan Flash Multimode Reader (Thermo Scientific, West Palm Beach, FL). Thioflavin T fluorescence at 482 nm was measured at 10 min interval by excitation at 440 nm. After the incubation, 5 μ L samples were taken out of each well for electron microscopy examination.

Acknowledgments

We thank Malcolm Capel, K. Rajashankar, Frank Murphy, Jonathan Schuermann, and Igor Kourinov at NE-CAT beamline 24-ID-C at APS and Daniel Anderson, Jason Navarro, Arthur Laganowsky, and Cong Liu for experimental help and discussions.

References

- Lucking CB, Brice A (2000) Alpha-synuclein and Parkinson's disease. *Cell Mol Life Sci* 57:1894–1908.
- Norris EH, Giasson BI, Lee VM (2004) Alpha-synuclein: normal function and role in neurodegenerative diseases. *Curr Top Dev Biol* 60:17–54.

3. Auluck PK, Caraveo G, Lindquist S (2010) alpha-Synuclein: membrane interactions and toxicity in Parkinson's disease. *Annu Rev Cell Dev Biol* 26:211–233.
4. Vekrellis K, Rideout HJ, Stefanis L (2004) Neurobiology of alpha-synuclein. *Mol Neurobiol* 30:1–21.
5. Uversky VN (2007) Neuropathology, biochemistry, and biophysics of alpha-synuclein aggregation. *J Neurochem* 103:17–37.
6. Spillantini MG, Goedert M (2000) The alpha-synucleinopathies: Parkinson's disease, dementia with Lewy bodies, and multiple system atrophy. *Ann N Y Acad Sci* 920:16–27.
7. Angot E, Steiner JA, Hansen C, Li JY, Brundin P (2010) Are synucleinopathies prion-like disorders? *Lancet Neurol* 9:1128–1138.
8. Galvin JE, Lee VM, Trojanowski JQ (2001) Synucleinopathies: clinical and pathological implications. *Arch Neurol* 58:186–190.
9. Uversky VN (2003) A protein-chameleon: conformational plasticity of alpha-synuclein, a disordered protein involved in neurodegenerative disorders. *J Biomol Struct Dyn* 21:211–234.
10. Jao CC, Der-Sarkissian A, Chen J, Langen R (2004) Structure of membrane-bound alpha-synuclein studied by site-directed spin labeling. *Proc Natl Acad Sci USA* 101:8331–8336.
11. Ulmer TS, Bax A, Cole NB, Nussbaum RL (2005) Structure and dynamics of micelle-bound human alpha-synuclein. *J Biol Chem* 280:9595–9603.
12. Burre J, Sharma M, Tsetsenis T, Buchman V, Etherton MR, Sudhof TC (2010) Alpha-synuclein promotes SNARE-complex assembly in vivo and in vitro. *Science* 329:1663–1667.
13. Chandra S, Gallardo G, Fernandez-Chacon R, Schluter OM, Sudhof TC (2005) Alpha-synuclein cooperates with CSPalpha in preventing neurodegeneration. *Cell* 123:383–396.
14. Burgoyne RD, Morgan A (2011) Chaperoning the SNAREs: a role in preventing neurodegeneration? *Nat Cell Biol* 13:8–9.
15. Makin OS, Serpell LC (2005) X-ray diffraction studies of amyloid structure. *Methods Mol Biol* 299:67–80.
16. Serpell LC, Berriman J, Jakes R, Goedert M, Crowther RA (2000) Fiber diffraction of synthetic alpha-synuclein filaments shows amyloid-like cross-beta conformation. *Proc Natl Acad Sci USA* 97:4897–4902.
17. Heise H, Hoyer W, Becker S, Andronesi OC, Riedel D, Baldus M (2005) Molecular-level secondary structure, polymorphism, and dynamics of full-length alpha-synuclein fibrils studied by solid-state NMR. *Proc Natl Acad Sci USA* 102:15871–15876.
18. Vilar M, Chou HT, Luhrs T, Maji SK, Riek-Loher D, Verel R, Manning G, Stahlberg H, Riek R (2008) The fold of alpha-synuclein fibrils. *Proc Natl Acad Sci USA* 105:8637–8642.
19. Chen M, Margittai M, Chen J, Langen R (2007) Investigation of alpha-synuclein fibril structure by site-directed spin labeling. *J Biol Chem* 282:24970–24979.
20. Jao CC, Hegde BG, Chen J, Haworth IS, Langen R (2008) Structure of membrane-bound alpha-synuclein from site-directed spin labeling and computational refinement. *Proc Natl Acad Sci USA* 105:19666–19671.
21. De Genst EJ, Guillemins T, Wellens J, O'Day EM, Waudby CA, Meehan S, Dumoulin M, Hsu ST, Cremades N, Verschueren KH, Pardon E, Wyns L, Steyaert J, Christodoulou J, Dobson CM (2010) Structure and properties of a complex of alpha-synuclein and a single-domain camelid antibody. *J Mol Biol* 402:326–343.
22. Robotta M, Braun P, van Rooijen B, Subramaniam V, Huber M, Drescher M (2011) Direct evidence of coexisting horseshoe and extended helix conformations of membrane-bound alpha-synuclein. *Chemphyschem* 12:267–269.
23. Georgieva ER, Ramlall TF, Borbat PP, Freed JH, Eliezer D (2010) The lipid-binding domain of wild type and mutant alpha-synuclein: compactness and interconversion between the broken and extended helix forms. *J Biol Chem* 285:28261–28274.
24. Varkey J, Isas JM, Mizuno N, Jensen MB, Bhatia VK, Jao CC, Petrova J, Voss JC, Stamou DG, Steven AC, Langen R (2010) Membrane curvature induction and tubulation are common features of synucleins and apolipoproteins. *J Biol Chem* 285:32486–32493.
25. Anderson VL, Ramlall TF, Rospigliosi CC, Webb WW, Eliezer D (2010) Identification of a helical intermediate in trifluoroethanol-induced alpha-synuclein aggregation. *Proc Natl Acad Sci USA* 107:18850–18855.
26. Thompson MJ, Sievers SA, Karanicas J, Ivanova MI, Baker D, Eisenberg D (2006) The 3D profile method for identifying fibril-forming segments of proteins. *Proc Natl Acad Sci USA* 103:4074–4078.
27. Kuhlman B, Baker D (2000) Native protein sequences are close to optimal for their structures. *Proc Natl Acad Sci USA* 97:10383–10388.
28. Goldschmidt L, Teng PK, Riek R, Eisenberg D (2010) Identifying the amyloidome, proteins capable of forming amyloid-like fibrils. *Proc Natl Acad Sci USA* 107:3487–3492.
29. Han H, Weinreb PH, Lansbury PT, Jr. (1995) The core Alzheimer's peptide NAC forms amyloid fibrils which seed and are seeded by beta-amyloid: is NAC a common trigger or target in neurodegenerative disease? *Chem Biol* 2:163–169.
30. Nelson R, Sawaya MR, Balbirnie M, Madsen AO, Riekel C, Grothe R, Eisenberg D (2005) Structure of the cross-beta spine of amyloid-like fibrils. *Nature* 435:773–778.
31. Wiltzius JJ, Landau M, Nelson R, Sawaya MR, Apostol MI, Goldschmidt L, Soriaga AB, Cascio D, Rajashankar K, Eisenberg D (2009) Molecular mechanisms for protein-encoded inheritance. *Nat Struct Mol Biol* 16:973–978.
32. Sawaya MR, Sambashivan S, Nelson R, Ivanova MI, Sievers SA, Apostol MI, Thompson MJ, Balbirnie M, Wiltzius JJ, McFarlane HT, Madsen AO, Riekel C, Eisenberg D (2007) Atomic structures of amyloid cross-beta spines reveal varied steric zippers. *Nature* 447:453–457.
33. Moon AF, Mueller GA, Zhong X, Pedersen LC (2010) A synergistic approach to protein crystallization: combination of a fixed-arm carrier with surface entropy reduction. *Protein Sci* 19:901–913.
34. Wiltzius JJ, Sievers SA, Sawaya MR, Eisenberg D (2009) Atomic structures of IAPP (amylin) fusions suggest a mechanism for fibrillation and the role of insulin in the process. *Protein Sci* 18:1521–1530.
35. Kim MW, Chelliah Y, Kim SW, Otwinowski Z, Bezprozvanny I (2009) Secondary structure of Huntingtin amino-terminal region. *Structure* 17:1205–1212.
36. Bodner CR, Maltsev AS, Dobson CM, Bax A (2010) Differential phospholipid binding of alpha-synuclein variants implicated in Parkinson's disease revealed by solution NMR spectroscopy. *Biochemistry* 49:862–871.
37. Jensen PH, Hager H, Nielsen MS, Hojrup P, Gliemann J, Jakes R (1999) alpha-synuclein binds to Tau and stimulates the protein kinase A-catalyzed tau phosphorylation of serine residues 262 and 356. *J Biol Chem* 274:25481–25489.

38. Ostrerova N, Petrucelli L, Farrer M, Mehta N, Choi P, Hardy J, Wolozin B (1999) alpha-Synuclein shares physical and functional homology with 14-3-3 proteins. *J Neurosci* 19:5782–5791.
39. Engelender S, Kaminsky Z, Guo X, Sharp AH, Amaravi RK, Kleiderlein JJ, Margolis RL, Troncoso JC, Lanthan AA, Worley PF, Dawson VL, Dawson TM, Ross CA (1999) Synphilin-1 associates with alpha-synuclein and promotes the formation of cytosolic inclusions. *Nat Genet* 22:110–114.
40. Eyal A, Szargel R, Avraham E, Liani E, Haskin J, Rott R, Engelender S (2006) Synphilin-1A: an aggregation-prone isoform of synphilin-1 that causes neuronal death and is present in aggregates from alpha-synucleinopathy patients. *Proc Natl Acad Sci USA* 103: 5917–5922.
41. Otwinowski ZMW (1997) Processing of X-ray diffraction data collected in oscillation mode. *Methods in enzymology*. New York: Academic Press, pp 307–326.
42. Kabsch W (1993) Automatic processing of rotation diffraction data from crystals of initially unknown symmetry and cell constants. *J Appl Crystallogr* 26:795–800.
43. Collaborative Computational Project, Number 4. (1994) The CCP4 suite: programs for protein crystallography. *Acta Crystallogr Sect D* 50:760–763.
44. McCoy AJ, Grosse-Kunstleve RW, Adams PD, Winn MD, Storoni LC, Read RJ (2007) Phaser crystallographic software. *J Appl Crystallogr* 40:658–674.
45. Emsley P, Cowtan K (2004) Coot: model-building tools for molecular graphics. *Acta Crystallogr Sect D* 60: 2126–2132.
46. Adams PD, Afonine PV, Bunkoczi G, Chen VB, Davis IW, Echols N, Headd JJ, Hung LW, Kapral GJ, Grosse-Kunstleve RW, McCoy AJ, Moriarty NW, Oeffner R, Read RJ, Richardson DC, Richardson JS, Terwilliger TC, Zwart PH (2010) PHENIX: a comprehensive Python-based system for macromolecular structure solution. *Acta Crystallogr Sect D* 66:213–221.